Electrochimica Acta 129 (2014) 266–275

Contents lists available at ScienceDirect

Electrochimica Acta

journal homepage: www.elsevier.com/locate/electacta

Thickness determination of electrochemical titanium oxide (Ti/TiO_2) formed in $HClO_4$ solutions

F.A. Filippin[a], O.E. Linarez Pérez[b], M. López Teijelo[b], R.D. Bonetto[c], J. Trincavelli[d], L.B. Avalle[e,*]

[a] Dep. Física. Facultad de Ciencias Exactas y Naturales, UNCa. Av Belgrano 300, 4700 Catamarca, Argentina.
[b] INFIQC-Departamento de Fisicoquímica, Facultad de Ciencias Químicas, Universidad Nacional de Córdoba, Ciudad Universitaria, 5000 Córdoba, Argentina.
[c] Centro de Investigación y Desarrollo en Ciencias Aplicadas Dr. Jorge Ronco, Facultad de Ciencias Exactas y Facultad de Ingeniería de la UNLP, La Plata, Argentina.
[d] Instituto de Física Enrique Gaviola (IFEG), Facultad de Matemática Astronomía y Física, Universidad Nacional de Córdoba, 5000 Córdoba, Argentina.
[e] Grupo de Electroquímica Experimental y Teórico. Instituto de Física Enrique Gaviola (IFEG), Facultad de Matemática Astronomía y Física, Universidad Nacional de Córdoba, 5000 Córdoba, Argentina.

ARTICLE INFO

Article history:
Received 18 December 2013
Received in revised form 12 February 2014
Accepted 19 February 2014
Available online 4 March 2014

Keywords:
Electrochemistry
Ellipsometry
EPMA
Oxide growth
TiO_2

ABSTRACT

Anodic Titanium oxide films were potentiodinamically grown on Ti foil and glass/Ti in 0.010 M $HClO_4$ at 50 mVs^{-1}. The current density-potential curves ($j-E$) showed that the oxide grows according to the physical model for high-field conduction. However, for final potential (E_f) higher than 1.5 V vs. Ag/AgCl (sat. KCl) the oxygen evolution reaction becomes more significant, and the formation of bubbles prevented or made more difficult the application of *in situ* techniques for the simultaneous study of the thickness and optical properties of the anodic layer. We developed a method based on electron probe microanalysis (EPMA) to calculate oxide thickness using *ex situ* ellipsometry as a reference technique. The normalized intensity of the O Kα peaks was measured for anodic oxides corresponding to E_f values from spontaneous oxide up to 50 V, where a linear relationship was observed for a narrower range of final potentials. This behaviour was studied with Monte Carlo simulations. After calibration with ellipsometric results, to take into account sample damage during the electron irradiation, EPMA was applied as a method for thickness determination at $E_f \geq 1.0$ V. Once the method was established, *ex situ* thickness determinations became independent of the preparation method of the oxide layer, which represents a comparative advantage against *ex situ* ellipsometry.

1. Introduction

In situ techniques provide a wide range of advantages regarding the study of the formation of thin oxide layers from a metal substrate [1] compared to *ex situ* procedures. However, when the reactions involved entail evolution of bubbles or dissolution-precipitation mechanisms of layer formation, the experimental requirements for determining thickness *in situ* are more demanding. In this situation, *ex situ* techniques are a convenient tool, making a wider range of potentials accessible. In the case of EPMA, once the technique is calibrated, the intensity of the O Kα characteristic line can be used to determine the thickness of electrochemical prepared oxides under different experimental conditions.

Electrochemical titanium oxide is formed mainly by galvanostatic, potentiostatic and potentiodynamic methods [2–14]. Poznyak et al. [15] investigated the morphology, structure and semiconducting properties of titanium oxide films formed by high-voltage pulsed discharge and compared them with the conventional galvanostatic anodization method, finding remarkably different physicochemical properties. Mazzarolo et al. [16] recently studied the anodic growth of titanium under the same conditions used for nanotube growth but in absence of fluoride ions. They determined the individual processes that occur during anodization up to 25 V in a two-electrode configuration using impedance measurements to calculate oxide thickness.

Anodic oxide thickness, mainly of valve metals, is usually calculated by charge integration from CVs obtained at different E_f values [17–20]. Pouilleau et al. [12] studied the structure and composition of TiO_2 films galvanostatically grown in 0.5 M H_2SO_4. They found thicknesses of between 23 and 62 nm for E_f of 5 V, 10 V and 20 V,

* Corresponding author.
E-mail address: avalle@famaf.unc.edu.ar (L.B. Avalle).

http://dx.doi.org/10.1016/j.electacta.2014.02.086
0013-4686/

being highly sensitive to the environment. They attributed the variations of interfacial capacitance to variations in the thickness of the outer TiO_2 layer, rather than to the modification of the composition of the surface compound. Their conclusions were based on surface analysis results, AFM and XPS. In previous works we studied anodic oxides formed in 0.1 M NaCl and compared them with each other and with respect to differences between thermal and sol-gel film growth [21–24]. It was found that the thickness of the oxide layer was the main factor determining the electrode response associated to the photocurrent quantum yields at $\lambda < 390$ nm. In the present work, anodic titanium oxide films were potentiodynamically formed on two different titanium substrates in 0.010 M $HClO_4$. The optical properties of the films prepared in a wide range of E_f values (up to 60 V) were obtained from *ex situ* ellipsometric measurements. The thickness of anodic oxide films for E_f values up to 10 V, was calculated assuming that oxide film grows as a single anisotropic layer with constant optical properties. These results were compared to the thickness values obtained by charge integration from current density-potential curves ($j - E$) (up to 1.5 V) and EPMA (up to 10 V). We have developed a comprehensive study of film thickness determination by EPMA, employing ex-situ ellipsometry as a reference technique for the calculation of anodic oxide thickness values. We have used Monte Carlo simulations to analyse the thickness range where proper results can be obtained considering the thin film hypothesis (TFH). This validated the use of the characteristic line of O Kα, detected under the irradiation of an electron probe, as a measure of oxide thickness.

2. Experimental

2.1. Materials

The working electrode was either a metallic titanium foil (purity 99.8%) or a glass/Ti, where the titanium metal thickness was 2 μm (glass sputtering targets prepared by Mateck GmbH). The glass/Ti samples were manually cleaned with a sequence of acetone-ethanol-water washing. The foil samples were sonicated for 10 min in MilliQ water and a thermal oxide was formed at 450 °C to isolate the back of the foil. The side of the electrode that has to be in contact with the electrolyte was polished with emery paper of different grades (1200 and 2500) and finished with 1 μm alumina. After mechanical polishing, two set of titanium foil samples were prepared: a) The samples labeled foil$^{(1)}$ were maintained under nitrogen gas (99.999% purity) before and after the electrochemical oxide was formed. b) The samples labeled foil$^{(2)}$ were stored one week before the electrochemical oxide was formed. The oxide film was grown potentiodynamically up to different E_f (1, 2, 3 V for both substrates and 4, 8, 9, 10, 30, 40, 50 and 60 V only for foils samples) at 50 mVs^{-1}. After oxide growth, the electrode was kept at the same E_f value for 15 min in order to stabilize the oxide film. A Ti/TiO_2 additional sample prepared from a titanium disk and electrochemically grown up to 30 V in 1% boric acid and 5% phosphoric acid was only studied by EPMA. This sample was used to check the reliability of this technique to determine the oxide layer thickness. Potential cycling between -1000 and 1500 mV (and also from -1000 to 0 V) at 50 mVs^{-1}, starting from the open circuit potential (ocp) of the electrode towards more negative values was performed. To ensure minimal differences between the different samples, a stabilized voltammogram was recorded for each electrode, and the $j - E$ profile was compared with a reference voltammogram. A difference of less than 5% was accepted. Otherwise, pretreatment of the substrate and all the described procedures were repeated. The electrolyte used in all measurements was a 0.010 M $HClO_4$ aqueous solution. The reference electrode was Ag/AgCl (saturated KCl). It was connected to the cell through a Luggin capillary filled with the same solution as in the main cell compartment. This arrangement minimized possible contamination of the solution by chloride anions. Oxygen free solutions were obtained by continuously purging the electrochemical cell with nitrogen gas (99.999% purity). All solutions, as well as glassware cleaning were prepared with water from a Milli-Q Millipore System. All chemicals were of analytical grade from Merck.

2.2. Cyclic Voltammetry (CV)

The electrochemical analyzer was an AUTOLAB-PGSTAT302N equipped with staircase scan module. In blank experiments, voltammetric curves were recorded at a scan rate (v) of 50 mVs^{-1} starting at the ocp and changing toward more negative values. The effect of double-layer charging was assessed by subtracting a given baseline from each steady state current voltammogram, j_{ss}. The results corresponding to the first voltammetric cycle are shown, otherwise it is indicated in the figure caption.

2.3. Ellipsometry

Optical measurements were performed ex-situ (in air) using a Rudolf Research rotating-analyzer type automatic ellipsometer (vertical type, 2000FT model), equipped with a 75 W tungsten lamp as the light source and a filter (546.1 nm). The incidence angle used for all experiments was 70.00°. The light reflected by the surface was passed through the rotating analyzer and into a photomultiplier tube (PMT) for detection. The sinusoidal output of the PMT was digitized by a HP microcomputer and the values of the ellipsometric angles Ψ and Δ were calculated by the computer from the three Fourier coefficients of the PMT signal. The PMT signal was averaged five times and the data were collected in operator-triggered mode. Ten measurements were taken for each sample. The optical data were fitted by using an anisotropic single-layer model, which assumes that oxide film growth takes place as a single anisotropic layer of constant optical properties growing on a flat bare titanium substrate. The fitting model uses the Simplex method [25] to minimize the error function

$$G = \frac{1}{m}\sum_i \left[(\Delta_i^{\exp} - \Delta_i^{calc})^2 + (\Psi_i^{\exp} - \Psi_i^{calc})^2) \right] \quad (1)$$

where the superscript "*calc*" denotes the values calculated from the model. No assumptions were made about the values of the optical properties of the oxide when fitting the experimental response, allowing the Simplex algorithm to vary the refractive index (n) and the extinction coefficient (k) in the normal (or ordinary; $\boldsymbol{n}_{ord} = n_{ord} - k_{ord}i$) and parallel (or extraordinary; $\boldsymbol{n}_{extr} = n_{extr} - k_{extr}i$) directions with respect to the surface of the anisotropic layer. Film thickness is an additional parameter that is also optimized in the fitting procedure; once the optical response is fitted in terms of the given model, both the optical properties and the thicknesses of the oxide films are obtained. The TiO_2 films were prepared by anodization of Ti foils, as described in section 2.1. Growth at high voltage took place using a two-electrode setup with a 173 EG&G PAR potentiostat/galvanostat (Princeton Applied Research, USA) coupled to a 175 EG&G PAR signal generator and a 7090A Hewlett Packard plotting recorder.

2.4. Scanning Electron Microscopy (SEM)

The surfaces of the titanium foils samples were studied with a field emission scanning electron microscope Carl Zeiss Σigma before and after anodic oxide formation, at the Laboratorio de Microscopía y Análisis por Rayos X (LAMARX) of the National University of Córdoba. Two different secondary electron detectors

were used: the in-lens type for high magnification and the Everhard Thornley detector for low magnification.

2.5. Electron Probe MicroAnalysis (EPMA)

The JEOL JXA 8230 microprobe available at LAMARX was used for three different purposes detailed in the following subsections.

2.5.1. Test of purity

To check the purity of the Ti film in the glass/Ti sample (without electrochemical treatment) both 12 and 20 keV electron beams were used to excite the sample with an energy dispersive spectrometer for detection. According to the results obtained with the standardless quantification algorithm implemented in POEMA [26], the only impurity detected was potassium with a mass concentration of 0.19 ± 0.03 %.

2.5.2. Determination of film thickness

When a flat sample is irradiated with an electron beam, the incident particles undergo multiple interactions with the atoms and are finally stopped within the material if it is thick enough (i.e., typically around one micrometer for electrons with incidence energy E_0 below 10 keV). Among the different interactions undergone by the electrons, an inner shell ionization can be followed by a radiative decay. The number of characteristic X-rays produced after a particular decay is greater for the more abundant elements in the sample. In the configuration studied here, a nanometric film of TiO_2 lies on a Ti substrate, which can be considered semi-infinite for the 4 keV electron beam used. With these ideas in mind, it can be stated that the thicker the oxide film, the more intense the O Kα peak detected. Moreover, it is reasonable to assume that peak intensity I will be proportional to the film mass thickness ρd for thin layers of mass density ρ and linear thickness d, so that self-absorption and electron scattering can be disregarded [27]. The relationship between I and film thickness was previously investigated by means of Monte Carlo simulations, as explained in section 3.4.1, in order to find a convenient value for E_0 and the thickness region of linearity between I and ρd. The software package PENELOPE was used [28] for this end. The samples formed by electrochemical oxide growth on metallic titanium foils at all E_f values, as described in subsection 2.1, were irradiated with a 4 keV electron beam. In view of the strong overlapping between the O Kα peak and the Ti-L lines, the measurement of spectra was carried out using the LDE1 crystal (with mylar window) of a wavelength dispersive spectrometer, whose high spectral resolution allows for a clear separation of the involved lines. A beam current I_0 of 80 nA was used, while the step size between channels was 10 μm, with a dwell time of 1.3 sec/channel, scanning a spectral range between 375 and 583 eV.

2.5.3. Study of the specimen current

The specimen current I_{spec} is defined as the electric charge conducted from the sample to the ground per unit of time. Taking into account that electrons from the incident beam can be backscattered from the sample, and considering also the emission of secondary electrons from the sample surface, the following can be written:

$$I_0 = I_{spec} + I_\eta + I_\delta \quad (2)$$

where I_η and I_δ are the electric currents due to electron backscattering and secondary electron emission, respectively. Eq. (2) can be normalized by I_0, so that,

$$1 = \frac{I_{spec}}{I_0} + \eta + \delta \quad (3)$$

where the so called backscattering and secondary electron coefficients η and δ, respectively, represent the number of electrons of each particular kind divided by the number of incident electrons. These coefficients depend on the mean atomic number of the sample and E_0. Particularly, η depends more markedly on the mean atomic number, while δ depends on E_0 and on surface characteristics. For these reasons, at constant values of E_0 and I_0, any change of the sample during the experiment would be evidenced by variations in I_{spec}. To study the stability of the sample during electron irradiation, the I_{spec} values were recorded throghout the experiment for two materials: bulk rutile (TiO_2), and a TiO_2 film anodically grown on a Ti substrate at E_f = 30 V. It must be clarified that this film was grown by a different method than the one described in subsection 2.1, but this fact does not affect the conclusions obtained as shown below.

3. Results and Discussion

3.1. Cyclic Voltammetry measurements

Fig. 1 shows $j-E$ profiles obtained for different Ti/TiO_2 foil$^{(2)}$ substrates, anodically oxidized in 0.010 M $HClO_4$ under potentiodynamic conditions with different E_f values. The physical model of the high-field conduction behavior of oxide growth can be used up to 1.5 V, as can be inferred from the steady state current observed after the onset in the $j-E$ curves, which is the characteristic kinetic behaviour of valve metals [29]. At more positive potentials than 1.5 V, the contribution from the oxygen evolution reaction becomes more significant, as it can be seen from the exponential-like current increase observed when the potential turns to higher positive values. Table 1 shows the potential values of the different electrodes for the onset of the mentioned processes. A large difference is observed when comparing the E^1_{onset} values of the samples laveled foil$^{(1)}$ and foil$^{(2)}$, indicating that the pre-treatment for foil$^{(2)}$ induced spontaneous oxide growth to a final thickness similar to the glass/titanium sample. Even though initial thickness for the two foil samples are different, the ΔE is 0.62 V for both electrodes and the potential window is remarkably large when compared to the glas/Ti electrodes. To keep track of the general characteristics of the initial thickness, two samples with E_f of 1.0 and 1.5 V were stored six months, and then the electrochemical oxide was grown up to E_f = 1.5 V. The current started increasing from 1.5 V in $j-E$ profiles, indicating that a spontaneous oxide was formed with a thickness corresponding at least to 1.5 V for both samples. Marino et al. [30] investigated the potentiodynamic formation of TiO_2 up to E_f = 5 V in NaH_2PO_4/Na_2HPO_4. They analysed the dissolution-reconstruction of different oxide films and calculated anodic oxide thickness by integration of the $j-E$ profiles. They found an anodization rate of 2.5 nmV^{-1} and estimated the initial thickness of the film (from air oxidation of the polished electrode) to be in the range ~ 1.9-3.0 nm. They identified the oxides present in the films by X-ray diffraction and found that for the film grown up to E_f = 1.5 V the diffractogram peaks corresponded to orthorhombic TiO_2, while for the films grown up to E_f> 3 V there were also peaks related to the

Table 1
Open Circuit Potential (E_{ocp}) from foil and glass/Ti/TiO_2/0.010 M $HClO_4$ interfaces. E^1_{onset} and E^2_{onset} refers to the start of oxide formation and oxygen evolution reactions, respectively. $\Delta E = |E^1_{onset}| - |E^2_{onset}|$. Electrode potential sweep rate: 50 mVs^{-1}. Reference electrode Ag/AgCl (sat. KCl). The thermal oxide was formed at 400 °C during 1 h.

Electrode	E_{ocp} (V)	E^1_{onset} (V)	E^2_{onset} (V)	ΔE
glass/Ti/TiO_2	0.29	0.89	1.0	0.11
foil$^{(1)}$	0.020	0.30	0.95	0.62
foil$^{(2)}$	0.30	0.85	1.5	0.62
glass/Ti/TiO_2 (thermally grown)	-0.080	-	-	-

foil$^{(1)}$ (electrochemical oxide inmediately formed after pre-treatment or kept in oxygen-free atmosphere)
foil$^{(2)}$ (stored one week before electrochemical oxide formation)

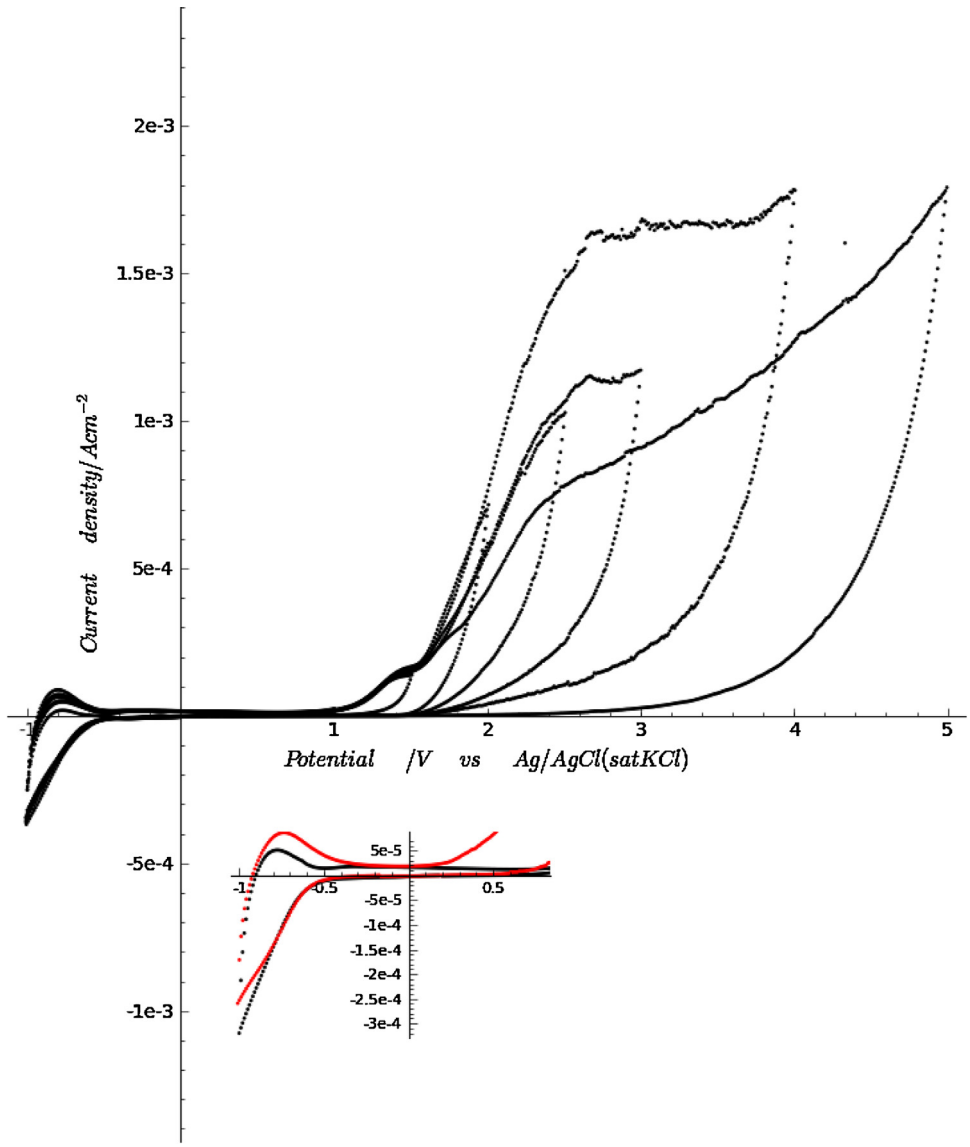

Fig. 1. Cyclic voltammogram curves of Ti/TiO_2 electrodes (each curve corresponds to a different foil(2)) in 0.010 M $HClO_4$ at 50 mVs^{-1}. The anodic oxide was potentiodinamically formed by increasing the positive potential limit (E_f / V vs Ag/AgCl (sat KCl)). Inset: $j-E$ profiles of foil(1) (red line) and foil(2) (black line) samples in the -1.0 V to 0.6 V range.

monoclinic mixed oxide Ti_3O_5. From the integration of current vs. time profiles (from the E^1_{onset} to E^2_{onset} potential region) the charge due to anodic oxide growth was calculated. Assuming a fixed stoichiometry of TiO_2, and using a value of 3.44 gcm^{-3} for the titanium oxide density (see section 3.3 below), the thickness values where obtained using the following equation

$$\Delta d_{ox} = \frac{M_{oxide} \quad Q_{oxide}}{nF\delta} \tag{4}$$

where M_{oxide} is oxide molar mass, Q_{oxide} oxide charge, δ is oxide density, n the number of electrons and F the Faraday constant. The procedure used to obtain the charge was as follows: a) the double-layer current density was substracted using the value at E^1_{onset} b) current density (current divided by the geometric area of the electrode) was integrated as a function of time for different E_f. c) thickness was calculated assuming perfect stoichiometry, four electrons, and oxide density of 3.44 gcm^{-3} (see section 3.3).

Jaeggi et al. [20] studied the potentiodynamic growth at 5 V/s, of titanium oxidefilms in 1 M sulfuric and phosphoric acid. From the $j-E$ profiles they observed that O_2 evolution did not occur in the phosphate-containing electrolyte at least up to 60 V. In our case, the O_2 evolution reaction started at the lowest potentials ever recorded when compared to any conditions reported in the literature. Surface techniques used to characterize anodic oxide films have demonstrated that there is a direct correlation between the defects in the TiO_2 crystalline lattice and the features observed in the CVs [12]. Galvanostatically formed anodic oxide in 0.5 M H_2SO_4 up to 5 V has a thickness of 23 $\pm$ 2 nm, 35 $\pm$ 4 nm at E_f = 10 V and 62 $\pm$ 5 nm at E_f = 20 V. Characteristic peaks of anatase and rutile were reported on Raman spectra of TiO_2 films, formed at low voltages (0 - 5 V) [31,8]. They proposed a three layer model by ellipsometry in which an intermediate TiO_x layer is inserted between a TiO layer in contact with the Ti substrate and the TiO_2 outer layer. It can be observed in the literature that the experimental conditions reported for anodic oxide growth contain high concentration of ionic species in solution (provided that anodic oxide formation was carried out in aqueous electrolytes). On the contrary, our experimental conditions correspond to a low concentration of a non-adsorbing electrolyte, where the characteristic features of the oxide surface/electrolyte interface observed in the -1.0 to 0 V range are more marked than in other electrolytes [21,22]. The inset in Fig. 1 shows the $j-E$ profiles in a narrowed range, where the current main features can be

associated only to the Ti(IV/III) processes for these characteristic potentials. This may indicate the absence of hydrogen-containing species that could be incorporated in the oxide [7], and/or low content of non-stoichiometric species in the TiO_2 lattice [7,32,33]. Ti_2O_3 may also be formed but in contact with water it is unstable and rapidly transforms to TiO_2 [34,35], which is more likely to occur at a low concentration of the electrolyte. The inset in Fig. 1 also shows differences during the negative potential scan, where the reduction of Ti(IV) (hydr)oxide species at the surface in contact with the electrolyte to Ti(III) (hydr)oxide species occurs and is related to the re-oxidation process obtained during the positive potential scan, this current being more pronounced for foil(1). The hydrogen adsorption-desorption process also takes place, demonstrating that there are several processes associated to this potential range. We consider that acording our experimental setup, the initial oxide thickness could be the main factor that determines the characteristic CV response of the first cycle, as is shown in the section 3.3. After anodic oxide growth, the films were subjected to several repetitive potentiodynamic cycles at 50 mVs^{-1} between -1.0 V and 0 V, showing that the electrochemical behavior of the passive electrodes remained unchanged (data not shown). Interestingly, the magnitude of the cathodic/anodic currents was different for each sample, but the observed shoulders appear always at the same potential values. The second range studied for these $j-E$ profiles was from 5.0 V to 60 V. During the formation process, the anodic TiO_2 films started dissolving from the foil edges towards the center of the electrode. This observation was visible from 10 V, where a dissolution-precipitation mechanism took place simultaneously with the formation of the TiO_2 lattice. The former led to particle deposition, which was observed by SEM, as is shown in the next section.

3.2. Differences observed in anodic oxides formed at the two substrates

The potentiodynamic formation-dissolution process of the oxide was studied at both substrates, with the surfaces analyzed by SEM and EPMA after different E_f values were applied. Fig. 2 shows SEM images of titanium foils before (Fig. 2a) and after (Fig. 2b, 2c and 2d) anodic oxide formation. Titanium foil displays a homogeneous surface at the initial state (Fig. 2a), where numerous stripes can be observed, most likely induced by mechanical polishing. Fig. 2b shows an SEM image of the electrode surface corresponding to the interface region with a magnification of 2,300x, where the right side corresponds to the non-immersed surface. Scanning towards the left, a different topography becomes evident and a well defined boundary edge is observed, where the brighter zone indicates the region where the anodic oxide was formed (corresponding to the electrode surface that was immersed in the electrolyte). Fig. 2c shows the anodic oxide zone within 10 μm from the interface. It can be observed that the stripes almost disappear, probably because the oxide growth rate is higher in those regions, and a stable long-range lattice of TiO_2 is formed. When the anodic oxide zone analyzed was located far from the interface (Fig. 2d), the SEM image showed a great number of deposited particles, the characteristic size of which ranged between a few micrometers to about 100 μm. These particles lay on a smoother surface compared to the surface corresponding to the other zones. The lamina-shaped particles could be interpreted as if they were formed from a side reaction that took place when the crystal was growing. Therefore, the film consists of a three-dimensional TiO_2 compact layer, where TiO_2 particles were deposited after the dissolution of a previously formed oxide and then a precipitation process occurred. Contrarily to the observations made by Jaeggi et al. [20], we found that the dissolution of anodic oxide is faster at the electrode edges for foil substrates. In addition, with increasing anodization potential i.e., increasing oxide thickness, pores cease to grow throughout the oxide, as was the case observed by Jaeggi et al. (data not shown). These facts could have a direct effect on anodic oxide thickness and its physicochemical properties. The *glass/Ti* sample has a regular texture composed by small grains ($\sim$ 500 nm) as shown in Fig. 3. The concentration of grain boundaries and the edges per unit area are visibly large and result in a high density when compared to the titanium foil surfaces. The local free energy of the anodic oxide formed on these grain boundaries, differs from that of bulk oxide, due to interfacial free energy contributions and the strength of the non-homogeneous electric field. As a result, these differences are more evident as the field becomes stronger, increasing the activity of the processes considered so far. This may be the main reason why oxide films could only be formed on titanium foil substrates with potentials higher than 5.0 V. The cross section of initial oxide and the anodic oxide corresponding to E_f = 3.0 V of these samples were also observed by SEM, but it was difficult to find a regular oxidized region after cutting the *glass/Ti/*TiO_2 sample which suggests that the films were fragile, with low adhesion to the substrate, and could easily become detached (break off) from the metal/oxide interface. Therefore, the differences observed between the two substrates with respect to the E_{ocp} values (see Table 1), could be a result of initial film morphology. The increase of thickness in this potential range, does not make a large difference in the morphological features of foil substrates, but in glass substrates the higher density of grains could produce an accelerated growth of the film through the joining of craters and pores. Nevertheless, the average thickness of the anodic films presented considerable local variations in thickness, especially in relation to the increase in voltage and variations in the proximity to the interface region. As a general trend, measurements showed that the films became thicker when E_f increased, as will be shown in the next section. Film thicknesses obtained from voltammperometric measurements demonstrates that there is a linear relationship between oxide growth and E_f when the double-layer and oxygen evolution currents are substracted from the j_T. With a naked eye, it can be observed that the anodic oxide formed from foils has less inhomogeneities at an anodization potential of 20 V compared to the corresponding oxide formed at higher potentials. Earlier works had always associated pores with nano-crystallites but recent studies demonstrated that the pores are formed by O_2 bubbles in oxides formed in H_2SO_4 and phosphate-containing electrolytes [20].

3.3. Ellipsometry

Ex-situ ellipsometry measurements for different samples were carried out after the anodic oxide was potentiodynamically formed at different E_f values. This procedure is less accurate than a CV measurement in which the same sample is used to sequentially form oxide of different thicknesses on its surface by applying an increasingly positive potential signal. The measurements were performed ex-situ since oxygen evolution produces light dispersion and interferes with the optical measurements at potentials higher than ca. 1.5-2 V. The oxides were grown in a wide range of potentials (from 1.0 V to 60 V) using a different sample (titanium foil(2)) for each E_f value. This procedure provides a wide range of oxide thickness. This, in turn, allowed a very good fitting of Ψ and Δ data values for obtaining reliable values of both optical properties and thickness values (see Fig. 4 below).

Fig. 4a shows the average Ψ and Δ angles recorded for the *Ti/*TiO_2*/air* interface after anodization to different E_f values. Although the crystalline TiO_2 oxides have highly anisotropic optical properties [36], all data sets could be reasonably fitted, with small error values, employing the anisotropic single layer model, which showed only a very slight anisotropy in the k values. The solid line in Fig. 4a represents the simulated curve for film growth

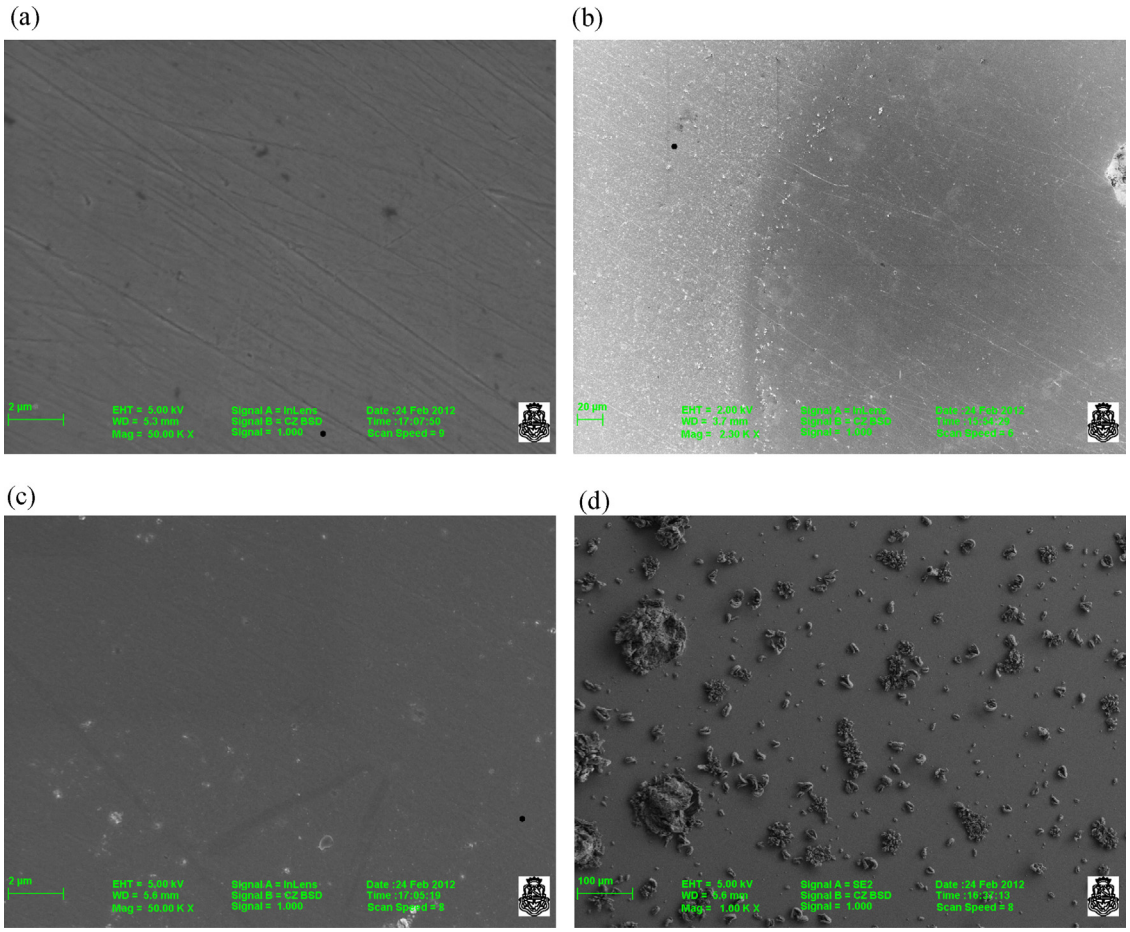

Fig. 2. SEM images of different magnifications of titanium foil electrodes. E_f=40 V vs Ag/AgCl (sat KCl) in 0.010 M $HClO_4$. a) initial oxide. b) interface region. c) anodic oxide zone within the 10 μm from the interface. d) anodic oxide zone more than 10 μm from the interface. The deposits observed in (d) correspond to TiO_2-particles.

up to a thickness of around 150 nm using the optical parameters obtained from the best fit: $n_{ord} = 2.38 - 0.004i$; $n_{extr} = 2.38 - 0.006i$. The value obtained for the refractive index of the anodic film (n_f = 2.38) is lower than those reported for tetrahedral anatase (n_α = 2.488; n_β = 2.561), tetrahedral rutile (n_α = 2.609; n_β = 2.900) or orthorhombic brookite (n_α = 2.583; n_β = 2.584; n_γ = 2.700) [36]. The lower value obtained for the refractive index of the anodic oxide formed in the present conditions as compared with known crystalline oxides can be attributed to hydration, the incorporation of anions or the lack of a crystalline structure [37,38]. On the other hand, the low values obtained for the extinction coefficients (k ≈ 0) indicate that the films are practically transparent, as found for other oxides formed on "*valve*" metals [37–39]. Thickness values, *d*, obtained also from the fitting procedure show a linear dependence with the formation potential (Fig. 4b). Under the anodizing and measurement conditions employed, an anodized rate α = 2.5 *nm* V^{-1} was obtained in the 1 V ≤ E_f ≤ 10 V range, which is of the same order of magnitude as those obtained by other authors ([19]

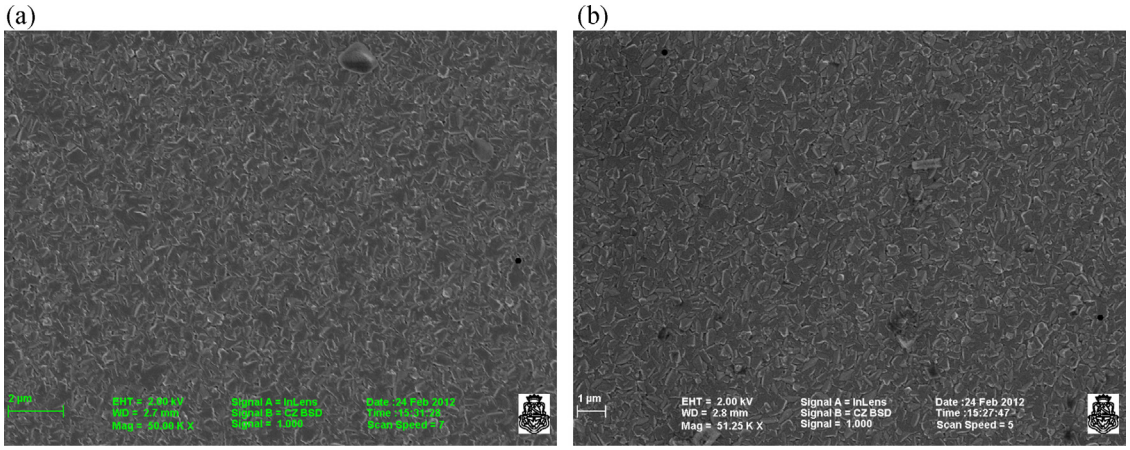

Fig. 3. SEM images of glass/Ti/TiO_2 electrodes. a) initial Ti/TiO_2. b) Ti/TiO_2 (E_f= 3 V).

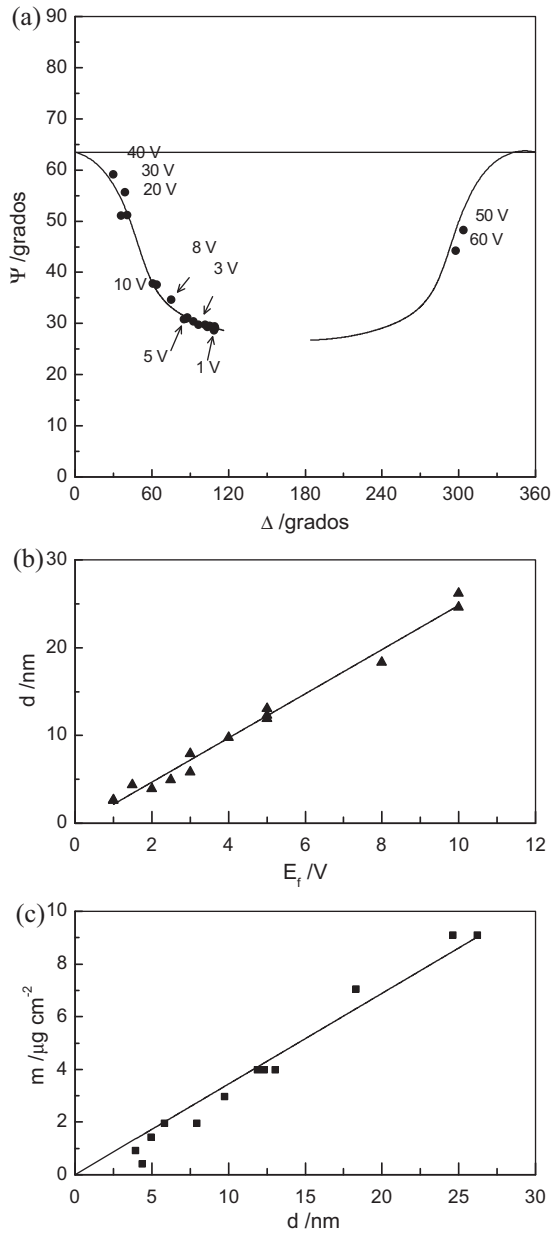

Fig. 4. a) Ψ-Δ ellipsometric response during the growth of TiO_2 films onto Ti foils up to different final potentials, E_f. The line represents the simulated curve connecting the anisotropic single-layer model with $n_{ord} = 2.38 - 0.004i$; $n_{extr} = 2.38 - 0.006i$. b) Thickness/E_f dependence obtained from the fitting procedure. c) Mass-thickness relationship.

and references therein). A value of 1.7 nm was estimated for the thickness of the initial TiO_2 film, from the extrapolation to the value of E^1_{onset}. This value for the spontaneously formed oxide is similar to that reported for other oxides [37–39]. The mass of TiO_2 per cm^2 generated during oxide formation was obtained from the anodic charge. The mass-thickness relationship (Fig. 4c) allowed then to estimate an oxide density value of $3.44\,g\ cm^{-3}$. This value is lower than those reported for crystalline TiO_2 (3.84; 4.26 and $4.17\,g\,cm^{-3}$ for anatase, rutile and brookite, respectively [36] indicating that anodic films are amorphous and highly hydrated, as can be concluded from the optical properties obtained. This agree with results obtained from X-ray diffraction for TiO_2 films formed in phosphate media, where crystalline orthorhombic TiO_2 were detected for potentiostatically aged titanium oxide films while an amorphous structure was found for cycled oxide films [40].

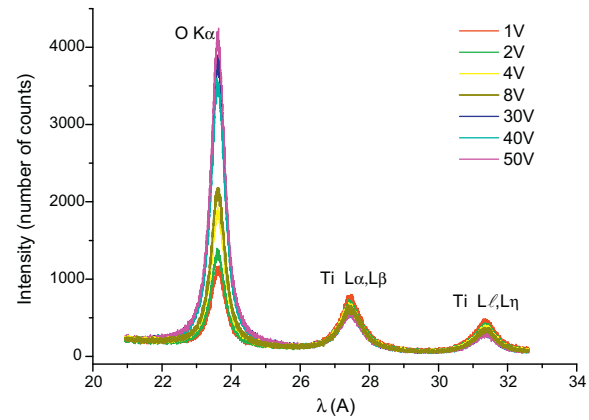

Fig. 5. X-ray emission of Ti/TiO_2 samples corresponding to different final potentials.

3.4. EPMA

Fig. 5 shows X-ray emission spectra as a function of photon wavelength λ of Ti/TiO_2 electrodes. The peak intensity of O Kα increases as E_f values increase. The intensity corresponding to the Ti Lα, β and $L_{l,\eta}$ doublets show an opposite trend. Both results were expected, since the thicker the oxide layer, the more oxygen atoms are expected to be available for the incoming electrons and less titanium atoms from the substrate can be ionized by the electron beam.

3.4.1. Determination of the growth rate

The net maximum values of normalized intensity (I) corresponding to the O Kα peaks were obtained after background subtraction by the beam intensity current (always around 80 nA). The acquisition time was 1.3 sec/channel for all the spectra. The results are plotted against E_f in Fig. 6. A linear behavior can be observed for the thinnest oxide layers, for which the effect of self-absorption and electron scattering can be neglected under a thin film hypothesis (TFH). This hypothesis of linearity between oxygen peak intensity and mass thickness was studied by Monte Carlo simulations of 4 keV electrons impinging on a TiO_2 film lying above a semi-infinite Ti substrate, using the software package PENELOPE2011. The corresponding results can be seen in Fig. 7. A linear fit, with zero intercept, can be fitted with a regression coefficient

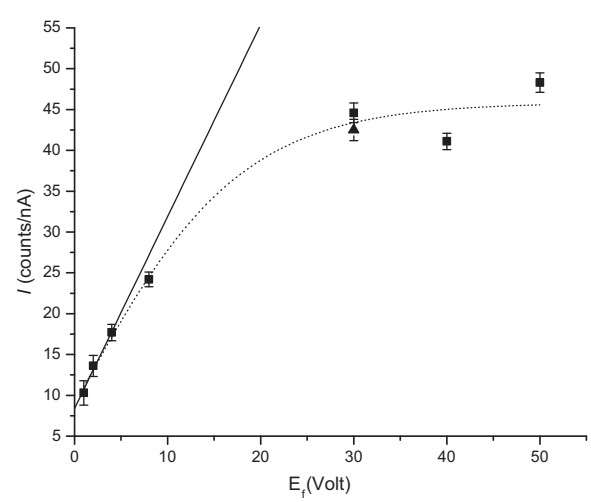

Fig. 6. Net maximum at the O-Kα peak normalized by the beam current as a function of E_f. Dots: experimental data; solid line: linear function fitted to the first three points; dashed line: fit to the whole range in the abscissa. Squares: Ti/TiO_2 prepared as explained in sec. 2.1; triangle: Ti/TiO_2 prepared using a different procedure.

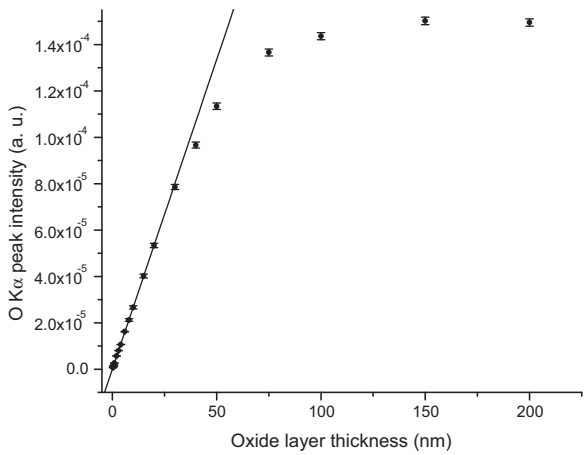

Fig. 7. Monte Carlo O-Kα peak intensities vs. TiO_2 layer thickness to check the thin film hypothesis.

of 0.99987, including data up to 30 nm. The observed linearity suggests that the TFH assumed should be met in this range. The linear function obtained in Fig. 6 can be expressed as:

$$I = 8.40 + 2.35E_f/V \quad (5)$$

The linear range of thicknesses d shown in Fig. 7, along with the results obtained by ellipsometry to relate d with E_f, allowed us to assume a linear behavior of I as a function of d in the range of validity of Eq. (5), i.e., up to E_f = 4 V. Assuming 1.7 nm for the spontaneous oxide (i.e. the thickness corresponding to the onset of 0.89 V), as suggested by the ellipsometry results, Eq. (5) evaluated in E_f = 0.89 V leds to 10.49 = c 1.7, where the proportionality factor c amounted to an increment ΔI of 6.2 nm^{-1}. On the other hand, Eq. (5) leads to ΔI = 2.35 E_f/V. From these results, a growth rate Δd = 0.38 ΔV nm/V was found. This figure was much lower than expected, which suggests that the sample was altered by the electron beam. In fact, a possible migration of oxygen atoms from the beam impact point would affect the growth rate determined by EPMA.

3.4.2. Oxide reduction by electron irradiation

Oxide reduction by electron irradiation was studied by monitoring the specimen current I_{spec}, as mentioned in section 2.5.3; the results of a Ti/TiO_2 electrode, where the oxide was grown anodically at E_f = 30 V, are shown in Fig. 8. Even when the electrolyte used to prepare this sample was different from the one employed for the other samples studied here, the decrease observed in I_{spec} depended only on the nature of the sample and not on its pretreatment. The fact that the nature of this sample was not strongly dependent on the preparation procedure is corroborated by the data plotted in Fig. 6, where its O Kα response (triangle) is indistinguishable from the corresponding data for the sample prepared as indicated in section 2.1 (squares). As can be seen in Fig. 8, after initial instability probably due to electric charging, a monotonous decrease of around 5% occurred, revealing a change in the sample, particularly, at its surface. It must be emphasized that the beam current I_0 was measured before and after the irradiation, and that it was markedly stable, even over periods of several hours. For this reason, the only magnitudes that can be thought to vary in the Eq. (3) of section 2.5.3 and to cause the variation in I_{spec} are the η and δ coefficients. Moreover, the region where backscattered electrons were produced was much larger than the source of secondary electrons. The latter corresponds to the surface, i.e., to the oxide layer, while the former mainly comprised the Ti substrate, which did not change during the experiment. Thus, the variation of I_{spec} can be attributed to a variation of δ, which, in turn, was due to the modification of the oxide layer at the beam impact point.

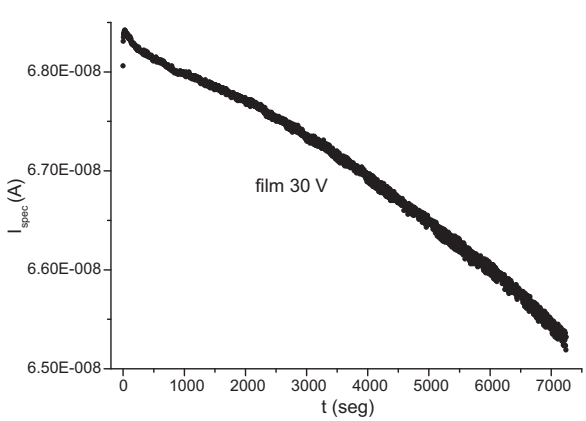

Fig. 8. Evolution of the specimen current during spectrum acquisition for Ti/TiO_2.

According to calculations made with aluminium, the production of secondary electrons is mainly caused by plasmon decay and by the excitation of conduction electrons [41]. Therefore, it is reasonable to consider that when the number of nearly free electrons increases in the irradiated material, i.e., the sample becomes a better conductor, the coefficient of secondary electrons will be greater. TiO_2 is an n-type semiconductor; when heated by the incident electron beam [42], atoms of the electronegative element (O) are loosened leaving an excess of atoms of the electropositive element (Ti). These extra atoms introduce additional energy levels from which it is easy for the electrons to jump to the conduction band. In particular, the conductivity σ varies with the temperature T according to $Aexp(-\epsilon/kT)$, where A is a constant, k is the Boltzmann constant and ϵ is the energy necessary to create an electron-hole pair. This behavior was experimentally verified by Earle [42] and by Padma et al. [43] for the particular case of TiO_2 films grown on pure Ti. In light of the previous discussion, it can be concluded that the observed decrease of I_{spec} can be attributed to a reduction of the oxide layer at the beam impact region. This result is in agreement with the work of Kern et al. [44]; they found that when a TiO_2 foil supported by a steel substrate is irradiated by electrons, a reduction to Ti_2O_3 is observed for a current density of 0.8 A/cm^2. It must be noted that a lower current density of 0.32 A/cm^2 was used here. The variation of I_{spec} shown in Fig. 6 allows to observe the reduction process during electron irradiation; as can be seen, reduction took place during the whole acquisition period, which comprised around two hours.

3.4.3. Correction of the EPMA results

Ex-situ ellipsometry measurements require a family of samples prepared by the same procedure involving several different thicknesses to be able of determine a relationship between the optical properties measured and the film thickness. On the other hand, to determine film thickness by EPMA, only the unknown sample is required, provided a calibration was previously performed with similar samples, independently of their method of preparation. Unfortunately, as discussed in subsection 3.5.2, the electron probe used to investigate the sample also produced its modification. For these reasons, it is of interest to find a relationship between the thicknesses obtained by EPMA, which involve a systematic error, and the more reliable data determined by ellipsometry. Thus, performing the adequate correction, a further determination by EPMA in a TiO_2 layer on a pure Ti substrate would produce reliable values of thickness, independently of the technique used to prepare the sample. The dashed curve shown in Fig. 6 represents a fit to all the data up to saturation, the expression obtained being

$$I = \alpha + \beta \tanh(\gamma E_f) \quad (6)$$

Table 2
Thicknesses obtained for different final potential of oxide formation (E_f) calculated from ellipsometry and EPMA techniques.

E_f(V)	d EPMA (nm)	d ellipsometry (nm)
1.0	1.1	2.0
2.0	5.1	4.5
4.0	10.2	9.5
8.0	19.0	19.5

with $\alpha = 8.976$, $\beta = 36.86$ and $\gamma = 0.05625V^{-1}$. On the other hand, as shown in subsection 3.3, the results obtained by ellipsometry exhibit a linear behavior between thickness and formation voltage in the 0-10 V range:

$$d = a + b(E_f - 0.89\,V) \tag{7}$$

with a = 1.7 nm and b = 2.5 nm/V. By eliminating the variable E_f, thickness can be related to the measured O Kα maximum as follows:

$$d = b\left[\frac{1}{2\gamma}\ln\left(\frac{1+\frac{I-\alpha}{\beta}}{1-\frac{I-\alpha}{\beta}}\right) - 0.89\,V\right] + a \tag{8}$$

The thicknesses obtained by EPMA and corrected (Eq. (8)) are presented in Table 2, along with the corresponding results obtained by ellipsometry (Eq. 7). The only values shown belong to the 0-10 V range, for which Eq. (7) is valid. The correction given in Eq. (8) produced results close to the ellipsometry values, except for the lowest voltage considered, for which the relative uncertainties are greater.

4. Conclusions

From the results reported here, a set of conclusions can be drawn concerning anodic oxide formation on titanium electrodes:

- The CV technique proved to be more useful than both, EPMA and ellipsometry, for determining differences in the thickness of the native oxide layer. The delay observed in the current onset for foil$^{(2)}$ and *glass*/*Ti*/TiO_2 electrodes, compared to foil$^{(1)}$ samples (which were kept under controlled atmosphere), indicates a thicker initial oxide. For the last samples an initial thickness of 0.2 nm was calculated considering their E^1_{onset} value, whereas a value of 1.7 nm was obtained for foil$^{(2)}$ samples by ellipsometry.
- The presence of a Ti(IV/III) process and the stability of the oxide layer under our experimental conditions were also well characterized by CV. The repetitive cycling in the -1.0 to 0 V potential range did not produce modifications in the characteristic response of (hydr)oxide surface groups, where both the anodic and cathodic charge transfer processes remained at the same peak potential values.
- High accuracy results were obtained by ellipsometry for the oxides electrochemically grown. The information about film thickness of foil and *glass*/*Ti*/TiO_2 substrates obtained by this technique corresponded to the average of a large area, averaging local fluctuations in film thickness. Moreover, the sample was not altered during the analysis. Finally, the ellipsometry technique requires a family of samples prepared by the same procedure involving several different thicknesses to be able of determe a relationship between the optical properties measured and the film thickness.
- The O Kα peak intensity increased as E_f increased, which was used as a characterization procedure. The analysis of the I_{spec} as a function of time allowed the detection of a modification in the original oxide caused by electron beam irradiation during sample analysis at the beam impact region, which resulted in a reduction of TiO_2 to Ti_2O_3. To overcome the obstacle of this modification of the sample during the study, a recalibration of the data was performed using the more accurate data from ellipsometry. After this correction, reliable results could be obtained by EPMA for single samples of TiO_2 films on titanium, that were prepared using different electrochemical conditions. The procedure of preparing a set of samples with the same optical properties was then avoided.
- Reliable results of titanium oxide electrochemically grown up to different thicknesses in 0.010 M $HClO_4$ were obtained by EPMA using *ex-situ* ellipsometry as a reference technique.
- There are many applications using EDMA that determine surface morphology, microstructure and chemical composition of anodic titanium oxide [45,46]. We developed a non conventional use for EPMA, where the thickness of thin films could be determined. However, limitations to respect of materials composed of several elements, produce x-rays with overlapping peak positions (by both energy and wavelength) that must be separated.
- In principle, the developed method can be applied to other stratified materials, provided the sample damage caused by the electron impact is not too high. The problem of a possible peak overlapping can always be overcame using a wavelength dispersive spectrometer and an adequate peak selection.

Acknowledgments

We are grateful for the support given by CONICET (Argentina). The support from Programa de Desarrollo Científico y Tecnológico 2011, Universidad Nacional de Catamarca, Secretaría de Ciencia y Tecnología, Consejo de Investigación. Código 02/G405 is also gratefully acknowledged. We thank Kyung Won Kang for providing one of the samples used in this paper. The authors also wish to thank language assistance by Mr. Vladimir Barbarena.

References

[1] M. Schneider, U. Langklotz, A Michaelis, Surface and Interface Analysis 45 (8) (2013) 1247–1251.
[2] I.A. Ammar, I. Kamal, Electrochimica Acta 16 (9) (1971) 1539–1553.
[3] C.K. Dyer, J.S.L. Leach, J. Electrochem. Soc. 125 (7) (1978) 1032–1038.
[4] A. Prusi, Lj. Arsov, Bala Haran, Branko N. Popov, J. Electrochem. Soc. 149 (11) (2002) B491–B498.
[5] S.V. Mentus, Electrochimica Acta 50 (2004) 27–32.
[6] M.V. Diamanti, M.P. Pedeferri, C.A. Schuh, Metallurgical and Materials Transactions A 39 (2008) 2143–2147.
[7] M. Schneider, S. Schroth, J. Schilm, A. Michaelis, Electrochimica Acta 54 (2009) 2663–2671.
[8] D.J. Blackwood, R. Greef, L.M. Peter, Electrochim. Acta 34 (1989) 875–880.
[9] D.J. Blackwood, L.M. Peter, D.E. Williams, Electrochim. Acta 33 (1988) 1143–1149.
[10] M.I. Rojas, M.J. Esplandiu, L.B. Avalle, E.P.M. Leiva, V.A. Macagno, Electrochim. Acta 43 (1998) 1785–1794.
[11] R. Beutner, J. Michael, B. Schwenzer, D. Scharnweber, J. R. Soc. Interface 7 (2010) S93–S105.
[12] J. Pouilleau, D. Devilliers, F. Garrido, S. Durand-Vidal, E. Mahé, Materials Science and Engineering B47 (1997) 235–243.
[13] Y.T. Sul, C.B. Johansson, Y. Jeong, T. Albrektsson, Med. Eng. Phys. 23 (5) (2001) 329–346.
[14] M.V. Diamanti, B. Del Curto, M. Pedeferri, J. Appl. Biomater. Biomech. 9 (1) (2011) 55–69.
[15] S.K. Poznyak, D.V. Talapin, A.I. Kulak, J. Electroanal. Chem. 579 (2005) 299–310.
[16] A. Mazzarolo, M. Curioni, A. Vicenzo, P. Skeldon, G.E. Thompson, Electrochimica Acta 75 (2012) 288–295.
[17] O.E. Linarez Pérez, V.C. Fuertes, M.A. Pérez, M. López Teijelo, Electrochem. Comm. 10 (2008) 433–437.
[18] H. Habazaki, M. Uozumi, H. Konno, K. Shimizu, P. Skeldon, G.E. Thompson, Corrosion Science 45 (2003) 2063–2073.
[19] A.G. Mantzila, M.I. Prodromidis, Electrochimica Acta 51 (2006) 3537–3542.
[20] C. Jaeggi, M. Parlinska-Wojtan, P. Kern, Thin Solid Films 520 (2012) 1804–1808, doi:10.1016/j.tsf.2011.08.092.
[21] F.Y. Oliva, L.B. Avalle, E. Santos, O.R. Cámara, J. Photochem. Photobiol. A: Chem. 146 (2002) 175–188.
[22] L.B. Avalle, O.R. Cámara, F.Y. Oliva, Journal of Electroanalytical Chemistry 585 (2005) 281–289.
[23] F.Y. Oliva, O.R. Cámara, L.B. Avalle, J. Electroanal. Chem. 633 (2009) 19–34.
[24] O.R. Cámara, L.B. Avalle, F.Y. Oliva, Electrochimica Acta 55 (2010) 4519–4528.

[25] Press W.H., B.P. Flannery, S.A. Teukolsy, W.T. Vetterling, Numerical Recipes: The Art of Scientific Computing, Cambridge, Cambridge, 1986.
[26] S. Limandri, R. Bonetto, V. Galvn Josa, A. Carreras, J. Trincavelli, Spectrochim. Acta B 77 (2012) 44–51.
[27] S. Limandri, M.A.Z. Vasconcellos, R. Hinrichs, J. Trincavelli, Phys. Rev. A 86 (2012), 042701 (10).
[28] F. Salvat, J. M. Fernndez-Varea, and J. Sempau, in Proceedings of the OECD/NEA. Data Bank, Issy-les-Moulineaux, France (OECD Publication, Paris, France, 2003).
[29] M. Dignam, J.O'M. Bockris, in: B.E. Conway, E. Yeager, R.E. White (Eds.), Comprehensive Treatise of Electrochemistry, vol.4, Plenum Press, New York, 1981, p. 247.
[30] C.E.B. Marino, E.M. de Oliveira, R.C. Rocha Filho, S.R. Biaggio, Corrosion Science 43 (2001) 1465–1476.
[31] A. Hugot Le Goff, Thin Solid Films 142 (1986) 193.
[32] M.P. Neupane, I.S. Park, S-J. Lee, K.A. Kim, M-H. Lee, T.S. Bae, Int. J. Electrochem. Sci. 4 (2009) 197–207.
[33] O.R. Cámara, C.P. De Pauli, M.C. Giordano, Electrochim. Acta 29 (1984) 1111.
[34] M. Pankuch, R. Bell, C.A. Melendres, Electrochim. Acta 38 (1993) 2777.
[35] L. Elfenthal, T. Patzelt, J.W. Schultze, O. Meyer, Mater. Sci. Eng. A 116 (1989) 71.
[36] D.R. Lide (Ed.), Handbook of Chemistry and Physics, 73rd ed., CRC Press, Boca Raton, 1992-1993.
[37] S. Gottesfeld, Electroanalytical Chemistry, vol.15, Marcel Dekker, New York, 1989, p. 143.
[38] O.E. Linarez Pérez, M.D. Sánchez, M. López Teijelo, J. Electroanal. Chem. 645 (2010) 143–148.
[39] M.A. Pérez, M. López Teijelo, Thin Solid Films 449 (2004) 138.
[40] E.M. De Oliveira, C.E.B. Marino, S.R. Biaggio, R.C. Rocha-Filho, Electrochem. Commun. 2 (2000) 254–258.
[41] L. Reimer, Scanning Electron Microscopy, Springer, 1985.
[42] M. Earle, Phys. Rev. A 61 (1942) 56–62.
[43] R. Padma, K. Ramkumar, M. Satyam, J. Mat. Sci. 22 (1987) 2083–2086.
[44] P. Kern, Y. Muller, J. Patscheider, J. Michler, J. Phys. Chem. B 110 (2006) 23660–23668.
[45] J.P. Schreckenbach, G. Mark, F. Schlottig, M. Textor, N.D. Spencer, Materials in medicine 10 (1999) 453–457.
[46] R. Akhter, S. Okawa, S. Nakano, M. Kobayashi, O. Miyakawa, Dent mater J. 19 (1) (2000) 10–21.